The flexible stalk domain of sTREM2 modulates its interactions with phospholipids in the brain

David Saeb[1], Emma E. Lietzke[1,2], Daisy I. Fuchs[1], Emma C. Aldrich[1], Kimberley D. Bruce[2], and Kayla G. Sprenger[1]

[1]Department of Chemical and Biological Engineering, University of Colorado Boulder, Boulder, CO, USA

[2]Department of Endocrinology, Metabolism, and Diabetes, University of Colorado Anschutz Medical Campus, Aurora, CO, USA

Abstract

The microglial surface protein Triggering Receptor Expressed on Myeloid Cells 2 (TREM2) plays a critical role in mediating brain homeostasis and inflammatory responses in Alzheimer's disease (AD). The soluble form of TREM2 (sTREM2) exhibits neuroprotective effects in AD, though the underlying mechanisms remain elusive. Moreover, differences in ligand binding between TREM2 and sTREM2, which have major implications for their roles in AD pathology, remain unexplained. To address these knowledge gaps, we conducted the most computationally intensive molecular dynamics simulations to date of (s)TREM2, exploring their interactions with key damage- and lipoprotein-associated phospholipids and the impact of the AD-risk mutation R47H. Our results demonstrate that the flexible stalk domain of sTREM2 serves as the molecular basis for differential ligand binding between sTREM2 and TREM2, facilitated by its role in stabilizing the Ig-like domain and altering the accessibility of canonical ligand binding sites. We identified a novel ligand binding site on sTREM2, termed the 'Expanded Surface 2', which emerges due to competitive binding of the stalk with the Ig-like domain. Additionally, we observed that the stalk domain itself functions as a site for ligand binding, with increased binding in the presence of R47H. This suggests that sTREM2's neuroprotective role in AD may, at least in part, arise from the stalk domain's ability to rescue dysfunctional ligand binding caused by AD-risk mutations. Lastly, our findings indicate that R47H-induced dysfunction in membrane-bound TREM2 may result from both diminished ligand binding due to restricted complementarity-determining region 2 loop motions and an impaired ability to differentiate between ligands, proposing a novel mechanism for loss-of-function. In summary, these results provide valuable insights into the role of sTREM2 in AD pathology, laying the groundwork for the design of new therapeutic approaches targeting (s)TREM2 in AD.

Introduction

Alzheimer's disease (AD) is a fatal neurodegenerative condition marked by progressive memory loss, cognitive decline, and impaired daily functioning[1]. Despite extensive research, the root causes remain unknown and curative treatments remain elusive. AD is hallmarked by the presence of extracellular amyloid-β (Aβ) plaques, intracellular neurofibrillary tau tangles, lipid droplet accumulation, and neuroinflammation[2,3]. Microglia, the brain's macrophages, play a pivotal yet complex role in AD pathology. While their phagocytic activity toward Aβ is considered neuroprotective, they also release cytokines that increase neuroinflammation, ultimately harming neighboring neurons and glia[4,5]. Two newly-approved monoclonal antibodies targeting Aβ, while transformative, have shown limited efficacy, only modestly slowing disease progression[6]. This underscores the need for a deeper understanding of the intricate interactions between the neuroimmune system and AD-relevant proteins.

At the forefront of this investigation is Triggering Receptor Expressed on Myeloid Cells 2 (TREM2), a transmembrane receptor expressed on microglial surfaces. TREM2 propagates a downstream signal through interactions with its co-signaling partner, DNAX-activating protein 12 (DAP12). Recent research highlights its crucial role in modulating microglial responses and maintaining brain homeostasis[7]. TREM2 contains an extracellular immunoglobulin (Ig)-like domain (19-130 amino acid (aa)), a short extracellular stalk domain (131-174 aa), a helical transmembrane domain (175-195 aa), and an intracellular cytosolic tail domain (196-230 aa)[8]. The Ig-like domain contains several ligand binding sites. These include a hydrophobic tip, which has a highly positive electrostatic potential and contains several aromatic residues and three complementarity-determining regions (CDRs), the latter of which (CDR2) also span part of a positively-charged basic patch known as the putative ligand interacting region, or 'Surface 1' (**Fig. 1**)[8–11]. Mutations in TREM2 correlate with altered risks of developing AD, with the R47H mutation, found on Surface 1, standing out as a significant genetic risk factor[12–14]. *In vitro* and *in silico* studies have consistently revealed that mutations, including R47H, destabilize TREM2's CDRs[8,15–17], exposing once-buried negatively charged residues[8,16] and disrupting homeostatic TREM2-ligand binding behavior[9,10,16,18].

TREM2 binds diverse anionic and lipidic ligands, including Aβ species[10,19,20], lipoproteins[10,21–23], nucleic acids[24], carbohydrates[25], and phospholipids (PLs)[9,18,26]—the focus of our study. PLs play a crucial role in lipid metabolism and maintaining brain homeostasis[27]. TREM2 clears excess PLs during demyelination and interacts with PLs when bound to lipoproteins with a core of neutral lipids surrounded by a monolayer of PLs, free cholesterol, and apolipoproteins[28,29]. Many PLs bind to TREM2, including phosphatidyl-choline (PC), -serine (PS), -inositol (PI), -glycerol (PG), -ethanolamine (PE), phosphatidic acid (PA), sphingomyelin (SM), cholesterol, and sulfatide[9,16,18,29]. PLs primarily bind to TREM2's hydrophobic patch and Surface 1, with varying affinities observed in different contexts[9,16,18]. Direct binding assays show stronger TREM2 binding to anionic moieties (PS, PE, PA) and weaker binding to PC and SM. Conversely, TREM2-expressing reporter cells reveal high TREM2 stimulation from PC and SM, especially with the $TREM2^{R47H}$ variant[18]. Collectively, however, these results emphasize TREM2's broad binding capabilities for PLs. Yet, one study suggested effective TREM2 stimulation by PLs may require co-presentation with other molecules, potentially reflecting the nature of lipoprotein endocytosis[30]. Another study observed minimal changes in TREM2-PL interactions despite

TREM2 mutations (R47H, R62H, T96K)[9]. Ultimately, there remains a major gap in understanding the mechanism for how PLs differentially interact with TREM2 and how this interaction is altered in disease-associated variants.

The activation of TREM2, mediated by the binding of ligands such as PLs, shapes key microglial functions, including proliferation, phagocytosis, and lipid metabolism. Notably, in pathological conditions, ligand-induced TREM2 activation triggers microglial phenotype switching to Disease-Associated Microglia (DAM), characterized by the activation of inflammatory, phagocytic, and lipid metabolic pathways[31]. Additionally, TREM2's extracellular domain can undergo cleavage from ADAM 10/17 sheddase at residue H157, yielding soluble TREM2 (sTREM2). The role and relevance of sTREM2 in disease pathology has been heavily debated[32]. In the cerebrospinal fluid of individuals with early-stage AD, elevated sTREM2 levels have been detected and linked to slower AD progression[33–35]. Further, there is a strong correlation between the levels of sTREM2 in the cerebrospinal fluid and that of Tau, however correlation with Aβ is inclusive. These findings have established sTREM2 as a long-time biomarker for AD diagnosis and progression[36–38].

Many studies have indicated a neuroprotective role for sTREM2 in disease pathology[39]. It has been suggested, for instance, that sTREM2 may function as a "dummy receptor" in AD states, preventing disease-associated ligands from binding TREM2[32]. Moreover, *in vivo* AD mouse models evaluating the therapeutic potential of recombinant sTREM2 have observed the suppression of microglial apoptosis, reduced Aβ plaque load, and improved learning and memory abilities[40,41]. More recent studies have indicated that sTREM2 not only serves as an activator for microglial uptake of Aβ but also directly inhibits Aβ aggregation[10,11,42]. Specifically, the binding of Aβ to TREM2 has been shown to increase shedding of sTREM2[42], which can then bind to Aβ oligomers and fibrils to inhibit their secondary nucleation[11,42]. Interestingly, the effect of R47H on Aβ aggregation is unclear, highlighting the need to study mechanistic aspects of ligand binding[11,42].

Some anionic ligands, including Aβ, predominantly bind to Surface 1 on TREM2. Intriguingly, recent observations revealed that Aβ binds to an alternative binding region, termed 'Surface 2', on sTREM2, situated opposite Surface 1 (**Fig. 1**). Surface 2 features a group of positively charged residues surrounded by acidic residues, creating a variegated electrostatic potential[11]. Herein, we aimed to unravel the molecular basis behind this functionally significant distinction in ligand binding between soluble and membrane-bound TREM2, utilizing molecular dynamics (MD) simulations. We focused on (s)TREM2-PL interactions, establishing a controlled framework to assess the impacts of various PL chemistries on ligand binding, specifically comparing the binding behavior of anionic PS and neutral PC. We hypothesized that the oft-overlooked flexible stalk domain of sTREM2, minimally explored in previous *in silico* studies, may play a pivotal role in mediating the observed variations in binding. Furthermore, we sought to understand the impact of the AD-risk mutation R47H on ligand binding, thereby unraveling fundamental roles of (s)TREM2 in AD pathology. To our knowledge, this study represents the second-ever application of MD to investigate sTREM2, totaling an unprecedented 17.2 μs of simulation time. Ultimately, this research may unveil new insights into the mechanistic and therapeutic roles of sTREM2 in AD.

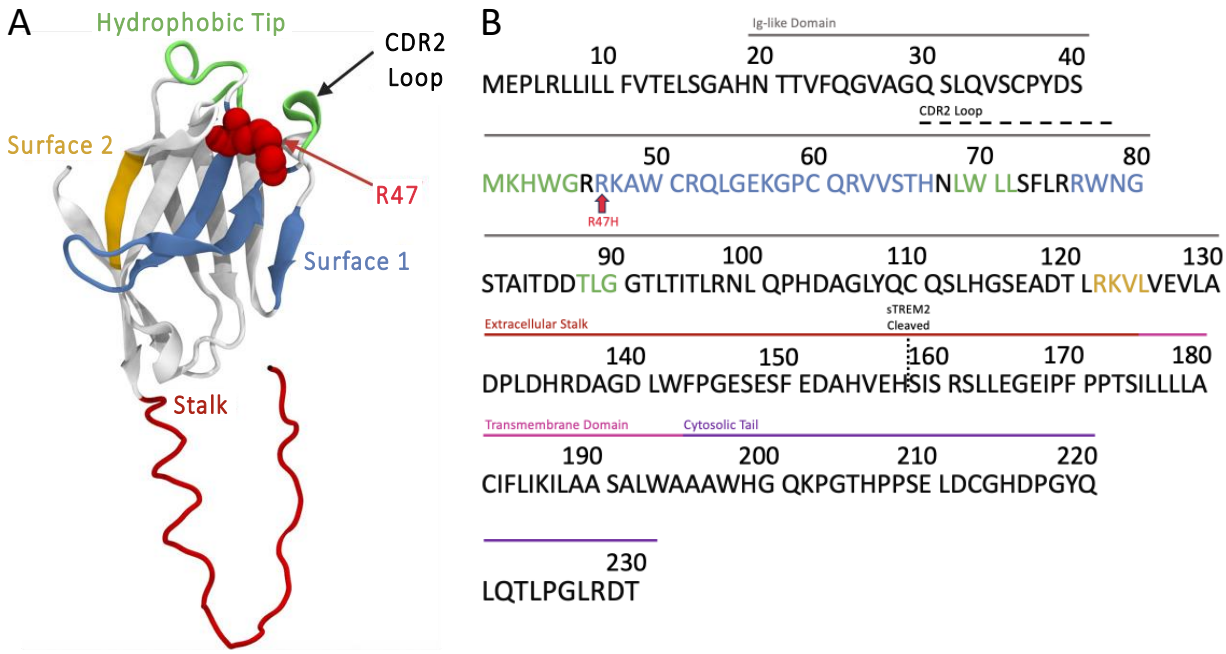

Figure 1. Overview of structural domains in sTREM2. (A) Pre-MD structure of sTREM2^{WT} and (B) Full sequence of TREM2, indicating significant structural domains.

Methods

Preparation of simulated structures

We employed the AlphaFold[43,44] model (AF-Q9NZC2-F1) as the initial structure for wildtype (WT) sTREM2 in our simulations, chosen for its inclusion of the unstructured flexible stalk domain. The partial stalk domain spans residues 130 through 157, while the Ig-like domain consists of residues 19 through 130. For WT simulations, we constructed two protein systems: one with just the Ig-like domain ("Ig^{WT}") and another containing both the partial stalk and Ig-like domain ("sTREM2^{WT}"). Similarly, two protein systems were constructed for the variant simulations: one with just the Ig-like domain containing the R47H mutation ("Ig^{R47H}") and another containing both the partial stalk and mutant Ig-like domain ("sTREM2^{R47H}"). In contrast to the use of the AlphaFold model for WT, we utilized a crystal structure of TREM2^{R47H} (Protein Data Bank (PDB) code 5UD8[16]), to which the unstructured stalk domain from the AlphaFold model was added using alignment tools in Visual Molecular Dynamics (VMD). Missing residues were incorporated into the TREM2^{R47H} Ig domain using MODELLER[45]. The initial molecular structures for the PLs, stearoyl-oleoyl-PC (SOPC) and stearoyl-oleoyl-PS (SOPS), were obtained from CHARMM-GUI[46–50], with each considered as a singular PL. All eight protein-ligand systems (Ig^{WT}, sTREM2^{WT}, Ig^{R47H}, and sTREM2^{R47H}, each with SOPC or SOPS) and six pure-component systems were solvated with explicit water and with counterions added as needed to neutralize the charge.

Molecular dynamics simulations

All proteins, PLs, and counterions were parameterized using the CHARMM36 force field[51,52], while the TIP3P model was used to describe water[53]. Prior to subsequent docking studies, each pure-component system underwent steepest-descent energy minimization, initially in vacuum and then in a solvated state. This was followed by a multi-step equilibration protocol, which included a 1 ns NVT equilibration simulation at 310K using the Bussi-Donadio-Parrinello thermostat[53], followed by a 1 ns NPT equilibration simulation at 310K and 1 bar using the same thermostat and Berendsen barostat[54]. Finally, production simulations were carried out at 310 K and 1 bar, utilizing the same thermostat and Parrinello-Rahman barostat[55]. The duration of the production simulations was 150 ns for each pure-component PL system and 1 μs for each pure-component protein system.

All simulations were conducted using the GROMACS MD engine[56]. The LINCS algorithm[57] was used to constrain bonds involving hydrogen atoms, and particle-mesh Ewald (PME) summations[58] were employed for calculating long-range electrostatics with a cutoff of 1.2 nm. Lennard-Jones interactions were evaluated up to 1.2 nm and shifted to eliminate energy discontinuities. Neighbor lists were reconstructed in 10-step intervals with a 1.4 nm cutoff. A timestep of 2 fs was implemented in all simulations, and periodic boundary conditions were applied in the x, y, and z directions. Configurations from these production simulations were used as inputs in ensuing docking calculations (see next section). After the docking calculations, we conducted additional 150 ns production simulations on the combined post-docking models, employing the same parameters as described above for the pre-docking production simulations.

Molecular docking calculations

For each of the four pre-docking, pure-component protein systems, we clustered the 1 μs production simulation trajectory using the gromos method implemented in GROMACS. Representative structures from the top two clusters in each case were selected and prepared for subsequent docking calculations using AutoDock Tools[59]. Docking calculations were carried out with AutoDock Vina[60,61], treating the proteins as rigid receptors. Given that AutoDock Vina employs a flexible ligand docking procedure, the final PL conformation from each pure-component simulation served as the ligand in the docking calculations. Grids with dimensions of 30 Å x 30 Å x 30 Å were constructed, redundantly covering the complete surface of each receptor protein. The exhaustiveness parameter for docking was set to eight. Docked complexes were analyzed based on the AutoDock score, the number of highly similar complexes, and biological relevance. Unique structures across grids and clusters for each ligand-receptor system were identified for post-docking MD simulations. From molecular docking, we obtained 7 unique SOPS/Ig^{WT} models, 5 SOPS/sTREM2^{WT} models, 5 SOPC/Ig^{WT} models, 6 SOPC/sTREM2^{WT} models, 4 SOPS/Ig^{R47H} models, 8 SOPS/sTREM2^{R47H} models, 6 SOPC/Ig^{R47H} models, and 7 SOPC/sTREM2^{R47H} models.

Trajectory analysis protocols

The Molecular Mechanics Poisson-Boltzmann Surface Area (MM-PBSA) approach was used to calculate PL-protein binding free energies, utilizing the gmx_MMPBSA implementation[62–64]. The analysis focused on temporal regions of the simulation trajectories where PL-protein complexes demonstrated stability, as indicated by relatively constant root-mean-square deviation

(RMSD) values for at least 50 ns. Over the same temporal regions, we calculated Interaction Entropy, as implemented in gmx_MMPBSA, to estimate entropic trends in PL binding[63,65]. Fractional occupancy values, characterizing the frequency and location of PL binding on each protein surface, were determined by calculating the fraction of simulation trajectory frames in which a given protein residue was within 4 Å of the PL across all simulations. We calculated conformational changes of the CDR2 loop using Visual Molecular Dynamics (VMD)[66] by measuring the distance between residues 45 and 70 at the tops of the CDR1 and CDR2 loops, respectively.

Results and Discussion

The partial stalk domain of sTREM2 stabilizes its Ig-like domain via binding to 'Surface 1'.

Prior TREM2 research identified an open CDR2 loop in R47H models, disrupting ligand binding to Surface 1[8,15,16]. Our 1-μs simulations consistently showed open CDR2 loops in both Ig^{R47H} and $sTREM2^{R47H}$ (**Fig. 2A**, slate blue and teal lines). Contrary to past experiments[15,16], Ig^{WT} transitioned from a closed to an open CDR2 loop midway through our simulation (**Fig. 2A**, pink line). To understand this result, we examined whether variation in the protonation state of histidine residue H43 in the CDR2 loop of Ig^{WT} and Ig^{R47H} could explain the observed variations in CDR2 loop dynamics. Initial protonation states (HSE in Ig^{WT}, HDE in Ig^{R47H}) were identified by GROMACS' pdb2gmx algorithm, based on optimal H-bonding conformations. Two additional 1 μs simulations of Ig^{WT} with the original protonation state (HSE) and three with the alternate state (HDE) were performed (**Fig. S1A**). The open CDR2 loop conformation was sampled in two out of the six trials, including the original Ig^{WT} simulation with the HSE protonation state for H43 and one trial with the HDE protonation state. This suggests that, while R47H consistently locks the CDR2 loop in an open state—as shown in past studies and **Fig. 2A—**the WT model's loop opening may be more stochastic and does not depend on H43's protonation state. We note that the CDR2 loop remained open in a 1 μs simulation of Ig^{R47H} with the alternate H43 protonation state (HSE).

Notably, $sTREM2^{WT}$ maintained a closed-loop conformation throughout the full 1 μs simulation (**Fig. 2A**, red line). This observation hints at a potential stabilizing effect on the CDR2 region, possibly attributed to the partial stalk domain present in $sTREM2^{WT}$ but which is absent in membrane-bound TREM2 (represented by Ig^{WT}). In the latter, stalk/Ig-like domain interactions are restricted by the connection of the stalk to TREM2's transmembrane domain. Given the potential stochastic nature of CDR2 loop opening (in the absence of R47H), we aimed to scrutinize this stabilization claim more rigorously through root-mean-square fluctuation (RMSF) calculations. These calculations involved the six Ig^{WT} simulations and the isolated Ig-like domain from the single $sTREM2^{WT}$ simulation ($sTREM2^{WT\text{-}Ig}$), assessed for each 1-μs trajectory (**Fig. 2B**). Compared to the six Ig^{WT} structures, $sTREM2^{WT\text{-}Ig}$ displayed reduced residue-level fluctuations across the entire Ig-like domain, suggesting broad stalk-induced stabilization. This effect was particularly evident around residues 66-77 and 84-90, encompassing portions of the hydrophobic tip and Surface 1, including the highly dynamic CDR2 loop region.

In light of these findings, we conducted a similar RMSF analysis to compare the dynamics of the isolated Ig-like domain from $sTREM2^{R47H}$ ($sTREM2^{R47H\text{-}Ig}$) against the two simulations of Ig^{R47H}

with the varying H43 protonation states (**Fig. S1B**). Similar to the WT model, the presence of the stalk led to substantially reduced residue-level fluctuations across the entire Ig-like domain of sTREM2$^{R47H\text{-}Ig}$, especially around residues 38-45 and 60-77. Collectively, these findings strongly suggest a stabilizing role for the partial stalk domain in sTREM2 Ig-like domain dynamics. This effect also appears to be largely independent of the degree of openness of the CDR2 loop, given the differences in CDR2 loop dynamics between sTREM2^{WT} and sTREM2^{R47H} shown in **Fig. 2A**.

We next aimed to elucidate the molecular basis for the stabilization of the Ig-like domain by the partial stalk domain of sTREM2. To this end, we calculated the RMSD of the Cα atoms in Ig^{WT} and sTREM2^{WT} (**Fig. 2C**), and in Ig^{R47H} and sTREM2^{R47H} (**Fig. 2D**), tracking their temporal positions relative to the respective energy-minimized configuration. The RMSD of each structure converged relatively quickly during the simulations. The Ig^{R47H} and Ig^{WT} simulations show behavior that mimics the CDR2 loop distances depicted in **Fig. 2A**. We observe a consistently low temporal RMSD profile for Ig^{R47H}, indicative of a persistently open CDR2 loop (inset panel **iii** of **Fig. 2D**). Similarly, the RMSD profile for Ig^{WT} is consistently low but increases slightly around 400 ns, signaling a transition from a closed to an open CDR2 loop (inset panels **iii** and **iv** of **Fig. 2C**). The CDR2 loop remains open for the remainder of the simulation, yet exhibits considerably larger RMSD fluctuations compared to the open CDR2 loop in Ig^{R47H}, indicating the R47H mutation likely imparts some stability to the open CDR2 loop.

Sharp initial increases in RMSD are observed with both sTREM2^{WT} and sTREM2^{R47H}. In both cases, the starting structures (inset panels **i** of **Figs. 2C-D**) exhibited a generally linear configuration of the stalk, potentially resembling its membrane-bound form. After the initial RMSD increases, the partial stalk domains were observed to consistently interact with the Ig-like domains of sTREM2^{WT} and sTREM2^{R47H} (inset panels **ii** of **Figs. 2C-D**). To identify the specific regions of the protein surface with which the partial stalk interacted during each simulation, we generated per-residue fractional occupancy maps characterizing the contact frequency (atom-atom distance within 4 Å) between the stalk and each residue in sTREM2^{WT} (**Fig. 2E**) and sTREM2^{R47H} (**Fig. 2F**). We observed a notable increase in the interaction frequency between residues on Surface 1 and the partial stalk domain of sTREM2^{R47H} compared to sTREM2^{WT}. This difference is likely due to the more open CDR2 loop of sTREM2^{R47H}, providing greater accessibility of Surface 1 residues for interaction with the stalk.

Given the highly negative overall charge of the stalk domain (-8), its recurrent interactions with the positively-charged residues in Surface 1 are perhaps intuitive. In addition to these interactions, the stalk domain in sTREM2^{WT} frequently interacted with residues 20-35, although with lower occupancy typically. While this region has not been directly noted in past experimental studies, it is located directly adjacent to residues highlighted in Surface 2 by Belsare et al[11]. Hence, we termed it the 'Expanded Surface 2'. Considering the diverse surface regions the stalk domain appears to interact with, and the overlap in many cases with known ligand binding sites on TREM2, these results may offer a potential mechanism for observed differences in ligand binding between sTREM2 and TREM2, which we explore in detail in the following section.

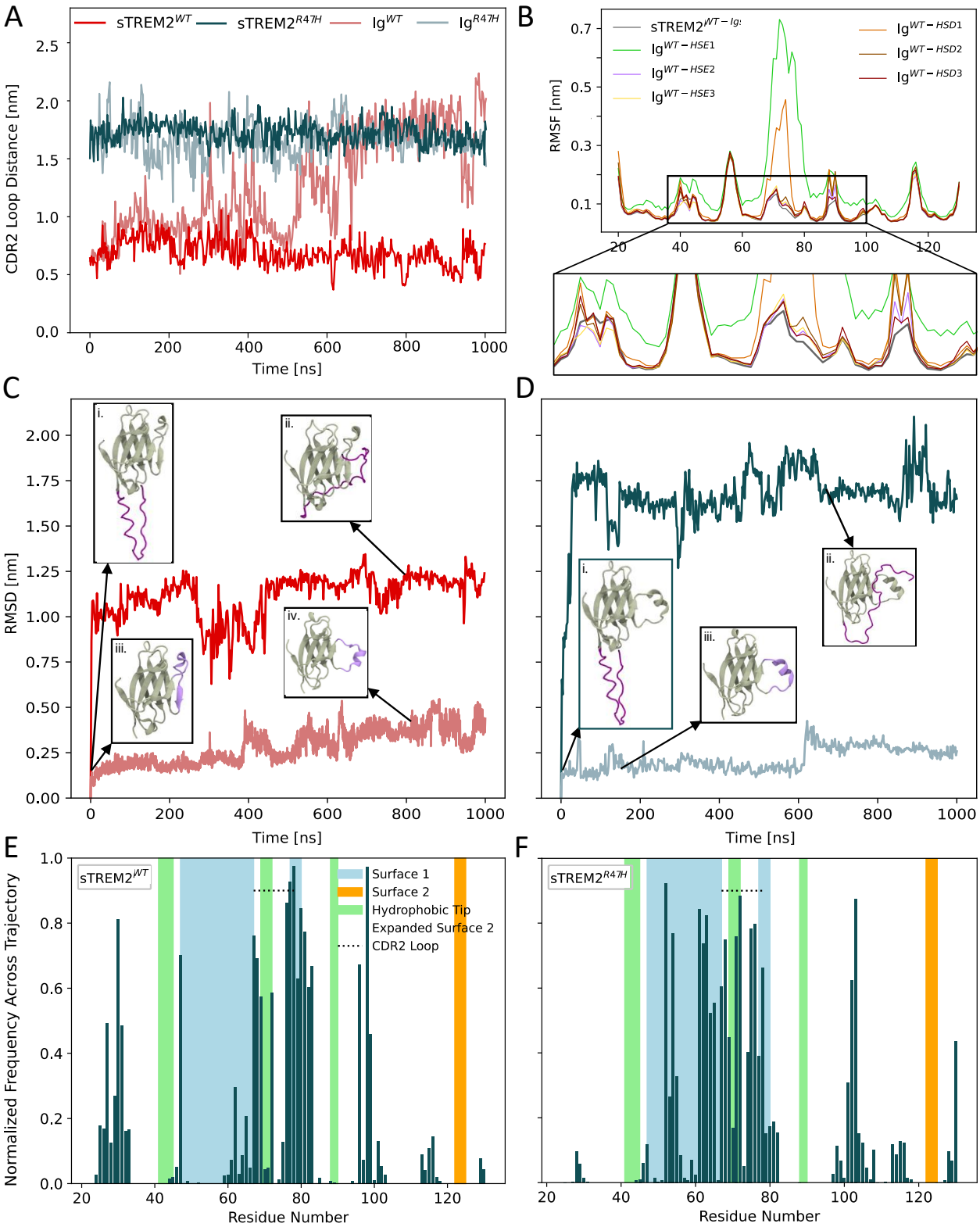

Figure 2. The stalk of sTREM2^{WT} stabilizes the Ig-like domain via binding to Surface 1. (A) Distance between CDR2 loop residues 45 and 70 vs. time for WT and R47H models of sTREM2 and TREM2 (Ig). (B) Temporally-averaged Cα-RMSF of the isolated Ig-like domain of WT sTREM2 (sTREM2$^{WT\text{-}Ig}$) vs. the Ig-like domain of TREM2 across six simulations (three trials

each with two different protonation states for H43 (see main text for details)). (C-D) Cα-RMSD of (C) WT and (D) R47H models of sTREM2 and TREM2 vs. time, with corresponding snapshots shown for the initial and equilibrated structures in each case. The stalk domain of sTREM2 is shown in dark purple, while the CDR2 loop of TREM2 is shown in light purple. (E-F) Normalized fractional occupancy of residues in the Ig-like domain of (E) sTREM2^{WT} and (F) sTREM2^{R47H} by the stalk.

sTREM2′s partial stalk domain modulates PL binding by promoting interactions with a new site on the Ig domain and creating an additional binding surface within the stalk itself.

In vitro studies investigating the molecular interactions of (s)TREM2 with ligands have been limited. One recent study found that sTREM2 demonstrated lower affinity for Aβ (of length 42 aa) compared to TREM2[10], suggesting potential differences in ligand binding between the two proteins. Another study presented a crystal structure featuring a TREM2 trimer bound by three PS molecules. This structure revealed broad PS binding to residues in the CDR2 loop and hydrophobic tip of TREM2[16]. While this study did not specifically explore PL/sTREM2 interactions, we hypothesized that similar differences in (s)TREM2 binding might be observed with PLs as seen with Aβ.

To test our hypothesis, we conducted 150 ns MD simulations of both Ig^{WT} and sTREM2^{WT} bound by the PLs stearoyl-oleoyl-PC (SOPC) and stearoyl-oleoyl-PS (SOPS) in various initial favorable docking configurations (see Methods for details). Subsequently, we analyzed the surface binding patterns of the PLs by determining the fractional occupancy of each protein residue, temporally averaged across all simulations for each protein/PL system. Across all four systems, we observed the highest occupancy by both PLs of residues located in the CDR2 loop and hydrophobic tip (**Figs. 3A-D**, primarily green regions), confirming earlier *in vitro* findings and validating our approach. Nevertheless, distinctions between the SOPS and SOPC models are evident, underscoring the influence of ligand charge on binding. Specifically, SOPS, being negatively charged, exhibited higher relative occupancy of the positively charged residues on Surface 1 compared to SOPC, which is neutrally charged (**Fig. 3A-B** vs. **3C-D**, resp., blue regions). Conversely, SOPC showed higher relative occupancy of residues in the hydrophobic tip than SOPS (**Fig. 3C-D** vs. **3A-B**, resp., green regions).

Upon comparing the fractional occupancy plots of the PL/sTREM2^{WT} simulations **(Fig. 3B** and **3D)** with those of the PL/Ig^{WT} simulations (**Figs. 3A** and **3C**), we observed a noticeable decrease in the relative occupancy of Surface 1, the hydrophobic tip, and specifically CDR2 loop residues in the PL/sTREM2^{WT} simulations compared to the corresponding Ig^{WT}/PL simulation. Instead, both PL/sTREM2^{WT} simulations revealed ligand binding to the newly defined Expanded Surface 2 (**Fig. 3B** and **3D**, light orange regions), to which the sTREM2^{WT} stalk was previously shown to bind, albeit with lower occupancy than Surface 1 residues (**Fig. 2E**). Significantly, there was an almost complete lack of PL binding to Expanded Surface 2 in the Ig^{WT} simulations. Collectively, these results suggest that Expanded Surface 2 serves as a secondary binding surface in sTREM2, becoming available for ligand binding when Surface 1 is occupied by the partial flexible stalk (and when Expanded Surface 2 is not *itself* bound by the stalk). Finally, we observed frequent interactions between both PLs and residues throughout the stalk domain of sTREM2^{WT} during

the simulations (**Fig. 3B** and **3D**, pink regions). This suggests that the stalk domain of sTREM2 may autonomously function as an additional binding site for diverse ligands.

We gained deeper insights into PL/(s)TREM2 interactions through visual analysis of our simulation trajectories using VMD and binding free energy calculations employing the MM-PBSA approach (see Methods). Representative snapshots from converged portions of the simulations for each protein/PL system (e.g., constant RMSD for at least 50 ns) are shown in **Fig. 3E-H**, alongside corresponding binding free energies. Among the WT systems, SOPS/Ig^{WT} exhibited the most favorable (lowest) binding free energy model, aligning with TREM2's known affinity for anionic ligands. Notably, SOPS and SOPC both directly interacted with Ig^{WT}'s CDR2 loop in the complexes with the lowest binding free energy (**Fig. 3E**, gray model and **Fig. 3G**, orange model).

In contrast, both SOPS/$sTREM2^{WT}$ and SOPC/$sTREM2^{WT}$ bind most favorable at the newly coined 'Expanded Surface 2' (**Fig. 3F**, orange model and **Fig. 3H**, purple model). This is explained by RMSF calculations (**Fig. S2**) and visual trajectory analysis which reveal heightened dynamics in the stalk domain, indicating that SOPS and, to a lesser extent, SOPC binding disrupts homeostatic stalk-Ig domain interactions. This disruption is further supported by the observation that, in the absence of a ligand, the stalk most frequently interacts with Surface 1 (**Fig. 2E**), where SOPS and SOPC bind in the absence of the stalk (**Fig. 3A**). Cumulatively, this indicates competitive binding between the PLs and the stalk domain for the CDR2 loop and Surface 1 given their similar, negative/amphipathic-charged natures.

To gain deeper insights into the thermodynamics of (s)TREM2/PL interactions, we performed Interaction Entropy (IE) calculations (see Methods). Although many free energy calculations overlook entropy, recent studies have emphasized its importance in providing a complete understanding of a system's Gibbs free energy[67,68]. IE calculations take into account changes in the ligand, protein, and solvent, and they efficiently estimate entropies directly from MD simulations. These calculations are particularly useful for assessing relative entropies[65]. Our results broadly indicate that the entropic contributions ($-T\Delta S$) are positive, with higher values for SOPS models compared to SOPC models; however, this difference is not statistically significant (**Fig. S3)**. Entropic loss upon ligand binding is attributed to the restriction of conformational freedom in the ligand, protein, and solvent[65,67]. The greater entropic loss observed for SOPS models suggests greater 'snugness' of binding[69], implying that binding is more enthalpically driven, particularly for SOPS. However, the applicability of our IE results is constrained by high standard deviations, likely due to the dynamic nature of TREM2-PL binding[70].

Uniquely, some PL/TREM2 complexes were observed to undergo rapid conformational changes in the CDR2 loop during the simulations, seemingly occurring on much shorter timescales than in the ligand-free simulations. These changes included the dynamic opening and closing of the CDR2 loop and alterations to its α-helical character (**Fig. 3E-H**). This suggests a potential mechanism for a dynamically responsive CDR2 loop in the context of ligand binding. Nevertheless, further experiments are essential to better understand the functional significance of CDR2 loop remodeling in response to ligand binding and to identify the circumstances in which it may occur.

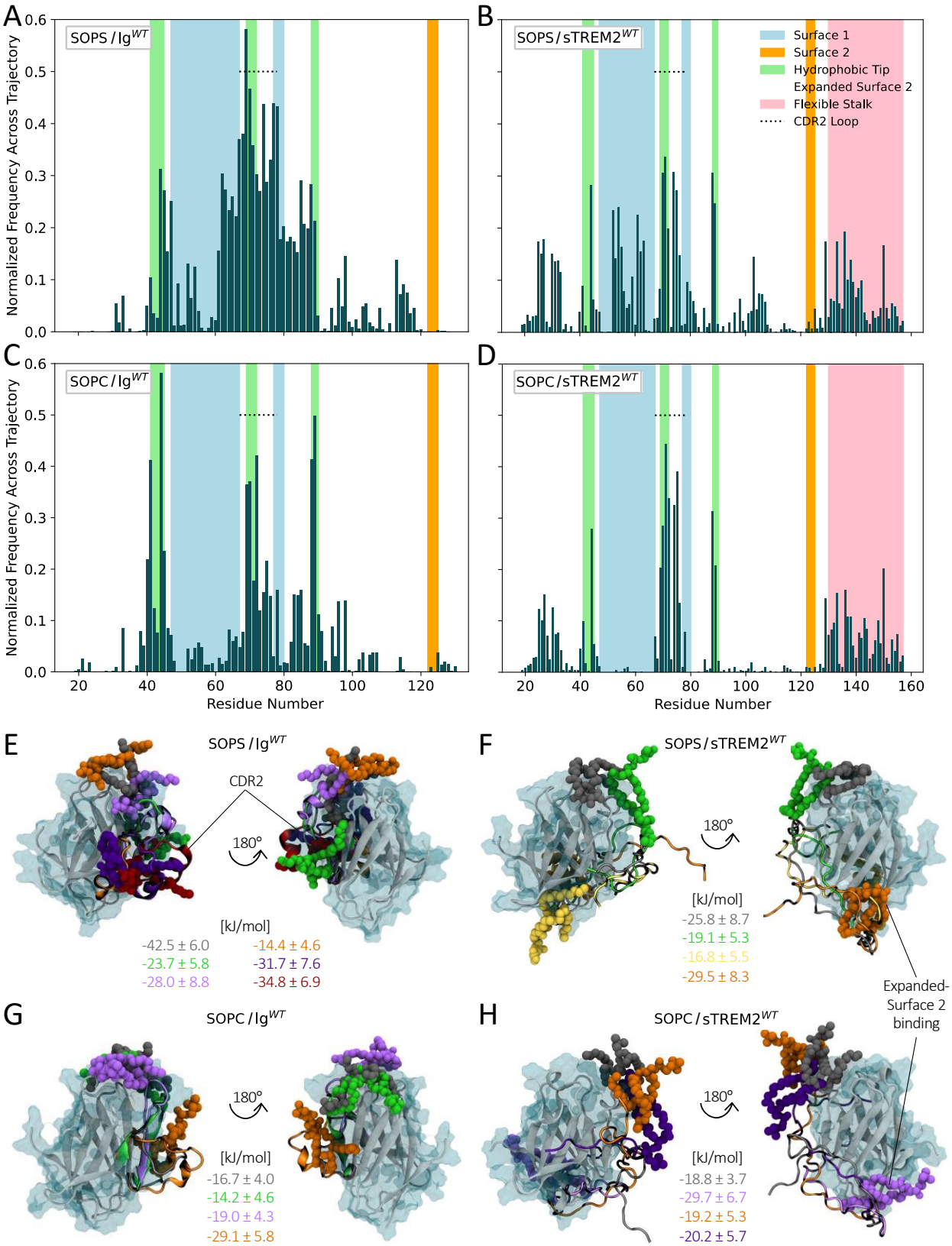

Figure 3. The stalk of sTREM2^{WT} modulates phospholipid binding. (A-D) Normalized fractional occupancy of residues in (A) Ig^{WT} by SOPS, (B) sTREM2^{WT} by SOPS, (C) Ig^{WT} by

SOPC, and (D) sTREM2^{WT} by SOPC, averaged across seven, five, five, and six 150 ns simulations, respectively. (E-H) VMD snapshots of representative structures from the PL/(s)TREM2^{WT} simulations, with PLs and corresponding complex binding free energies shown in matching colors.

The AD-risk mutation R47H diminishes ligand discrimination by and binding to the Ig-like domain of (s)TREM2, while sTREM2's stalk domain partially restores overall ligand binding.

To investigate the roles of (s)TREM2 in disease pathology, we examined PL binding in the presence of the AD-risk mutation R47H. Previous studies have suggested that the decreased ligand-binding capabilities of TREM2^{R47H} may underlie its observed loss-of-function[9,10,16,18]. Notably, one study showed reduced reporter cell activity of TREM2^{R47H} compared to TREM2^{WT} when binding anionic lipids such as PS, while no significant difference was observed in their binding to PC[18]. Separately, sTREM2^{R47H} and sTREM2^{WT} were shown to bind Aβ and inhibit fibrillization to a similar extent[11].

Upon examining the fractional occupancy plots of the PL/(s)TREM2^{R47H} simulations, we observed broadly similar patterns in binding to the Ig-like domain, regardless of the presence of the stalk or PL charge (**Fig. 4A-D**). Across all four simulations, PLs predominantly occupied the CDR2 loop and Surface 1 of the Ig-like domain. This uniformity in binding contrasts sharply with the previously discussed behavior observed in the PL/(s)TREM2^{WT} simulations (**Fig. 3A-D**), where notable differences in binding to SOPS and SOPC were observed for both Ig^{WT} and sTREM2^{WT}, as well as between the two proteins for a given PL. These results suggest that the presence of R47H diminishes the ability of Ig^{R47H} and sTREM2^{R47H} to distinguish between crucial brain-based ligands, proposing a novel mechanism for loss-of-function due to AD-risk mutations.

Compared to the PL/(s)TREM2^{WT} simulations, all four PL/(s)TREM2^{R47H} simulations demonstrated marked reductions in PL binding to the hydrophobic tip. These differences likely arose from structural impacts on the hydrophobic tip region due to the more open and rigid nature of the nearby CDR2 loop in the presence of R47H, altering the ligand binding properties of the hydrophobic tip. Furthermore, variations in binding between the stalk and Ig-like domain due to R47H (**Fig. 2E-F**) also likely contributed to these PL binding changes. Additionally, diminished binding to Expanded Surface 2 was observed for PL binding to sTREM2^{R47H}.

Compensating for these reductions in binding, increased PL binding to Surface 1 was observed in all four R47H simulations, along with enhanced PL binding to the flexible stalk of sTREM2^{R47H}. These results provide further support for the notion that the sTREM2's stalk domain functions as an independent ligand binding site. Moreover, these results suggest the stalk domain may possess an inherent ability to 'rescue' sTREM2 deficiencies in ligand binding to the Ig-like domain due to disease-associated mutations, offering an explanation for sTREM2's neuroprotective role in AD. Indeed, this could explain why, as mentioned earlier, the presence of R47H does not significantly reduce sTREM2^{R47H}'s ability to bind Aβ and inhibit fibrillization to the same degree as sTREM2^{WT}.

Following the methodologies used to evaluate the PL/(s)TREM2^{WT} simulations, we conducted visual analysis of our trajectories paired with binding free energy calculations. Representative

structures with corresponding binding free energies are shown in **Fig. 4E-H**. Broadly, binding free energy trends align closely with those observed for the WT complexes (**Fig. 3E-H)**, with the SOPS/Ig^{R47H} complexes again exhibiting the lowest (most favorable) energy model (**Fig. 4E**). Unlike the WT complexes, however, these results do not indicate competitive binding between SOPS and the partial stalk region, evidenced by highly favorable binding in the CDR2/Surface 1 region for PL/(s)$TREM2^{R47H}$ models. This may be a result of the persistently open CDR2 loop which alters surface accessibility and stalk dynamics.

The results show that across all models, sTREM2 and TREM2 bind PS more favorably than PC, affirming previous findings that TREM2 favors anionic ligands[30]. However, these differences are not statistically significant. Additionally, this analysis shows no significant difference or trend in binding free energies for PS/WT complexes compared to their PS/R47H equivalents, contrasting with previous experimental findings that the R47H mutation reduces TREM2's affinity for endogenous ligands[10,16,18] (**Fig. 4I**). Similar to WT models, we observe that for R47H models, SOPS binding poses exhibit higher average entropic contributions than their SOPC counterparts. These observations suggest that weaker ligand binding does not comprise the entire mechanism for signaling deficits in the R47H variant. Broadly, these results suggest that differences in binding across a range of ligands, (s)TREM2 variants, and between sTREM2 and TREM2 are governed by accessibility of protein surface residues and ligand binding patterns, factors which extend beyond mere differences in binding affinities.

Lastly, we noted an intriguing difference in the stability of the CDR2 loop between Ig^{R47H} and Ig^{WT}. Throughout the majority of the simulations, regardless of PL presence, the CDR2 loop in Ig^{R47H} remained stable in an open conformation, contrasting with the Ig^{WT} simulations where the CDR2 loop exhibited dynamic opening and closing in response to PL binding. Thus, in addition to directly impacting ligand affinities and impairing the ability to differentiate between ligands, the R47H mutation may inhibit the CDR2 loop's ability to dynamically respond to ligand binding, thereby preventing physiological TREM2 signaling. However, further studies of the TREM2-DAP12 complex are needed to understand how ligand binding to the Ig-like domain propagates signaling and how these mechanisms may be disrupted in the R47H variant.

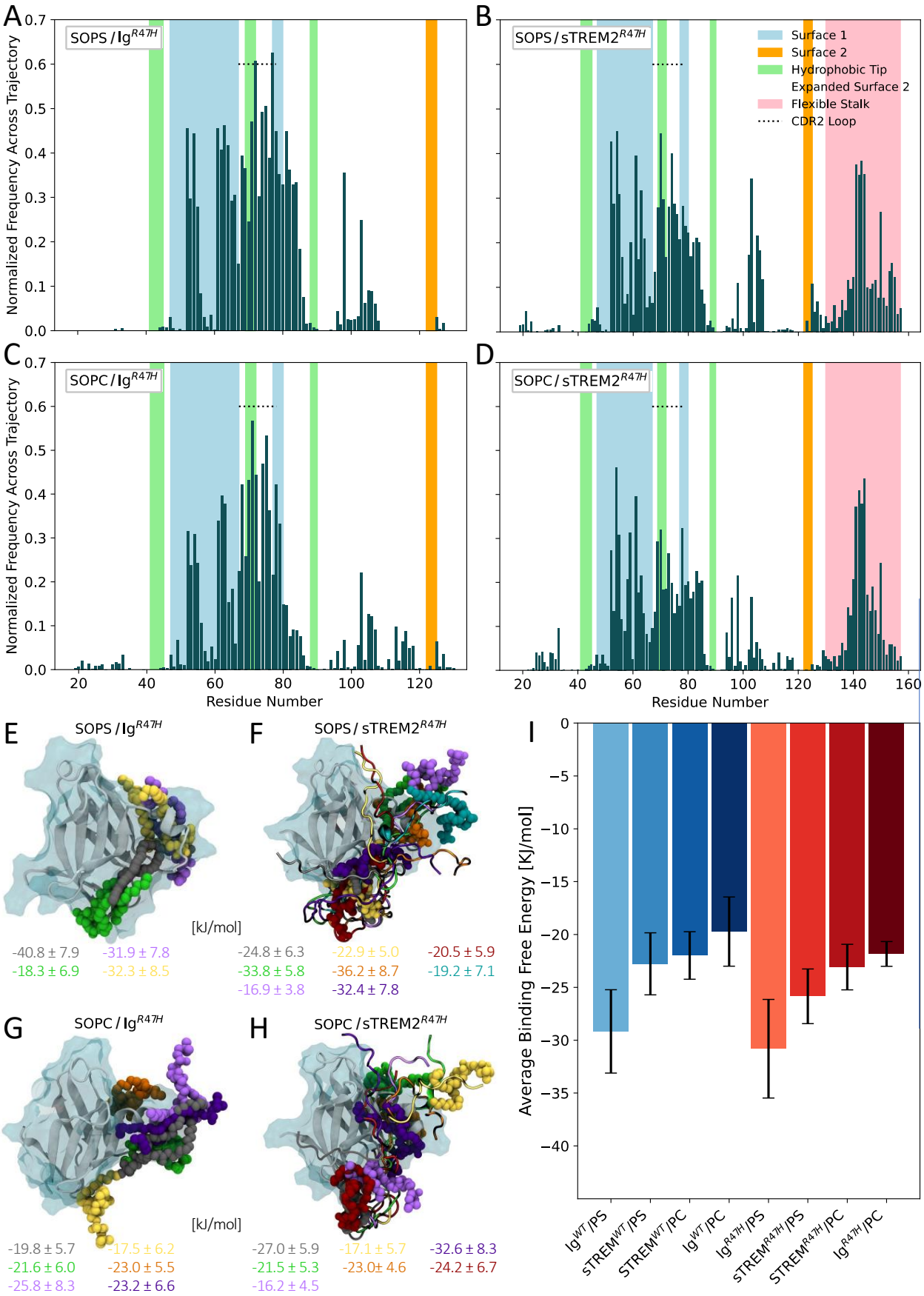
A
SOPS / Ig^{R47H}
B
SOPS / sTREM2^{R47H}
Surface 1
Surface 2
Hydrophobic Tip
Expanded Surface 2
Flexible Stalk
CDR2 Loop
C
SOPC / Ig^{R47H}
D
SOPC / sTREM2^{R47H}
Normalized Frequency Across Trajectory
Residue Number
E
SOPS / Ig^{R47H}
F
SOPS / sTREM2^{R47H}
[kJ/mol]
-40.8 ± 7.9
-31.9 ± 7.8
-18.3 ± 6.9
-32.3 ± 8.5
-24.8 ± 6.3
-22.9 ± 5.0
-20.5 ± 5.9
-33.8 ± 5.8
-36.2 ± 8.7
-19.2 ± 7.1
-16.9 ± 3.8
-32.4 ± 7.8
G
SOPC / Ig^{R47H}
H
SOPC / sTREM2^{R47H}
[kJ/mol]
-19.8 ± 5.7
-17.5 ± 6.2
-21.6 ± 6.0
-23.0 ± 5.5
-25.8 ± 8.3
-23.2 ± 6.6
-27.0 ± 5.9
-17.1 ± 5.7
-32.6 ± 8.3
-21.5 ± 5.3
-23.0± 4.6
-24.2 ± 6.7
-16.2 ± 4.5
I
Average Binding Free Energy [KJ/mol]
Ig^{WT}/PS
sTREM^{WT}/PS
sTREM^{WT}/PC
Ig^{WT}/PC
Ig^{R47H}/PS
sTREM^{R47H}/PS
sTREM^{R47H}/PC
Ig^{R47H}/PC

434

Figure 4. R47H mutation decreases ligand discrimination but increases binding to the flexible stalk. (A-D) Normalized fractional occupancy of residues in (A) Ig^{R47H} by SOPS, (B) $sTREM2^{R47H}$ by SOPS, (C) Ig^{R47H} by SOPC, and (D) $sTREM2^{R47H}$ by SOPC, averaged across four, seven, six, and eight 150 ns simulations, respectively. (E-H) VMD snapshots of representative structures from the PL/(s)$TREM2^{R47H}$ simulations, with PLs and corresponding complex binding free energies shown in matching colors. (I) Comparison of the binding free energies averaged across all WT and R47H models for each PL/protein system. Errors bars represent the standard error of the mean.

Discussion and Conclusions

Main Conclusions

We utilized long-timescale MD simulations to investigate relevant structural domains of sTREM2 and TREM2, along with their interactions with key PLs in the brain. Through the analysis of RMSF, RMSD, and surface occupancy calculations, we established the flexible stalk domain of sTREM2 as the molecular basis for differential ligand binding between sTREM2 and TREM2. This difference in binding arises from the stalk's role in stabilizing the Ig-like domain and altering the ligand-accessibility of its surface residues. By integrating free energy, interaction entropy, and ligand occupancy calculations, we quantified the energetics of these interactions, confirming the presence of an alternate ligand binding site on $sTREM2^{WT}$, which we termed the 'Expanded Surface 2'. The binding of PLs to this site results from the competitive binding of the flexible stalk domain to Surface 1 on the Ig-like domain. These stalk-Ig-like domain interactions were disrupted in the presence of the AD-risk mutation R47H and entirely absent in the Ig (TREM2) models, indicating occupancy of Expanded Surface 2 occurs solely with $sTREM2^{WT}$. These observations underscore our conclusion that, rather than (or in addition to) its previously conceived role as a dummy receptor for TREM2, the flexible stalk domain confers sTREM2 with unique ligand binding preferences and patterns that facilitate distinct endogenous functions compared to TREM2.

Furthermore, we found that the stalk domain itself serves as an independent site for ligand binding, with heightened PL occupancy observed in the presence of R47H compared to the wildtype model. This suggests that the stalk domain may have the capacity to partially 'rescue' dysfunctional ligand binding to the Ig-like domain of sTREM2 caused by disease-associated mutations like R47H. Moreover, our observations for both sTREM2 and TREM2 indicate that R47H-induced dysfunction may result not only from diminished ligand binding but also an impaired ability to discriminate between different ligands in the brain, proposing a novel mechanism for loss-of-function. In summary, the findings of this study reveal the endogenous structural and dynamical mechanisms of (s)TREM2, a critical component in AD pathology. These insights offer new fundamental knowledge that can serve as guiding principles for the design of future therapeutics, paving the way for potential advancements in AD treatment strategies.

Ideas and Speculation

Our findings suggest that loss-of-function in sTREM2 and TREM2 occurs not only through experimentally observed loss of binding affinity, but also through a change in binding patterns

and a loss of ligand discrimination capacity. Altered ligand binding may hinder the ability of TREM2 and its co-signaling partner DAP12 to transmit signals across the cell membrane. This deficiency implicates an impaired microglial response to ligand binding as a key mechanism for dysfunction in AD. Pathologically, this would lead to reduced lipid uptake[71], diminished Aβ plaque clearance[19], decreased microglial activation[71], and inhibited intracellular lipid metabolism[72]. Previous studies speculate that reduced microglial lipid metabolism can trigger neurotoxic activation states or loss of neuroprotective functions[73]. Furthermore, the inability to discriminate among PLs may result in an invariable response from microglia when presented with diverse ligands. While PC is the most abundant PL in cell membranes, PS expression on the outer membrane leaflet increases in apoptotic cells, acting as a damage-associated signal[74]. Failure to differentiate between these PLs may lead to chronic over-activation of microglia, or at the very least, loss of endogenous protective functions.

Recently, monoclonal antibodies targeting TREM2 have emerged[75–77], designed to bind to the stalk region, above its cleavage site[76,77]. Consequently, the primary binding epitope of at least one of these antibodies also resides on sTREM2. Notably, this antibody also reduces the shedding of sTREM2[77]. It is conceivable that treatment with this and similar antibodies may compromise the endogenous function of sTREM2, given that the stalk, a domain our study has identified as functionally significant, may be sequestered by the antibody. This may ultimately result in off-target effects for these therapeutics and prompts a consideration of how to separately target sTREM2 and TREM2.

Limitations

As with all models, particularly computational ones, it is crucial to recognize their limitations. In our study, the initial positions of PLs bound to (s)TREM2 were determined exclusively by AutoDock Vina. To mitigate potential bias from the docking process, we conducted MD simulations on all unique structures observed in the top 20 docked models. Rigorous, yet computationally efficient free energy calculations remain a challenge for computational protein-ligand studies. Despite employing the latest MM-PBSA free energy calculation algorithms and novel interaction entropy calculations, achieving statistical significance for many of the trends we observed that align with experiments remained challenging. This difficulty was further compounded by our approach of averaging statistics across multiple models of PLs docked to different initial binding locations on (s)TREM2. While this approach was intended to holistically capture PL/(s)TREM2 interactions, it effectively diluted our sample size against any specific epitope, potentially impacting the statistical significance of our findings. Future studies could address these challenges by utilizing larger sample sizes of independent MD simulations and more intensive energy calculations as computational power and resources continue to advance.

Moreover, our study, like previous investigations of TREM2, assumed that the Ig-like domain is representative of membrane-bound TREM2. This assumption overlooks potential contributions from the membrane, membrane-bound flexible stalk domain, DAP12, or TREM2 glycosylation. Ultimately, more biologically representative simulations of membrane-bound TREM2 are warranted to test this assumption. Additionally, it is unlikely that PLs are presented as individual soluble ligands in the brain in an *in vivo* setting. Instead, they are more likely co-presented with other components in lipoproteins or in contexts such as demyelination, cell debris, or Aβ. This co-presentation would influence the charge and steric profiles of lipid presentation. While our

study provides valuable insights and fills existing knowledge gaps, further research is necessary to fully understand TREM2 binding in more biologically relevant ligand-binding contexts.

Acknowledgements

This work utilized the Alpine high performance computing resource and Blanca condo computing resource at the University of Colorado Boulder. Alpine is jointly funded by the University of Colorado Boulder, the University of Colorado Anschutz, and Colorado State University. Blanca is jointly funded by computing users and the University of Colorado Boulder.

References

1. Alzheimer & Association. *Alzheimer's Association 2024 Alzheimer's Disease Facts and Figures*. https://www.alz.org/media/Documents/alzheimers-facts-and-figures.pdf (2024).
2. Kinney, J. W. *et al.* Inflammation as a central mechanism in Alzheimer's disease. *Alzheimer's and Dementia: Translational Research and Clinical Interventions* vol. 4, (2018).
3. Farmer, B. C., Walsh, A. E., Kluemper, J. C. & Johnson, L. A. Lipid Droplets in Neurodegenerative Disorders. *Frontiers in Neuroscience* vol. 14, (2020).
4. Miao, J. *et al.* Microglia in Alzheimer's disease: pathogenesis, mechanisms, and therapeutic potentials. *Frontiers in Aging Neuroscience* vol. 15, (2023).
5. Franklin, H., Clarke, B. E. & Patani, R. Astrocytes and microglia in neurodegenerative diseases: Lessons from human in vitro models. *Progress in Neurobiology* vol. 200, (2021).
6. Tobeh, N. S. & Bruce, K. D. Emerging Alzheimer's disease therapeutics: promising insights from lipid metabolism and microglia-focused interventions. *Frontiers in Aging Neuroscience* vol. 15, (2023).
7. Deczkowska, A., Weiner, A. & Amit, I. The Physiology, Pathology, and Potential Therapeutic Applications of the TREM2 Signaling Pathway. *Cell* vol. 181, (2020).
8. Dean, H. B., Roberson, E. D. & Song, Y. Neurodegenerative Disease–Associated Variants in TREM2 Destabilize the Apical Ligand-Binding Region of the Immunoglobulin Domain. *Front Neurol* **10**, (2019).
9. Kober, D. L. *et al.* Neurodegenerative disease mutations in TREM2 reveal a functional surface and distinct loss-of-function mechanisms. *Elife* **5**, (2016).
10. Kober, D. L. *et al.* Functional insights from biophysical study of TREM2 interactions with apoE and Aβ1-42. *Alzheimer's and Dementia* **17**, 475–488 (2021).
11. Belsare, K. D. *et al.* Soluble TREM2 inhibits secondary nucleation of Aβ fibrillization and enhances cellular uptake of fibrillar Aβ. *Proc Natl Acad Sci U S A* **119**, (2022).
12. Jonsson, T. *et al.* Variant of TREM2 Associated with the Risk of Alzheimer's Disease . *New England Journal of Medicine* **368**, (2013).
13. Guerreiro, R. *et al.* TREM2 Variants in Alzheimer's Disease . *New England Journal of Medicine* **368**, (2013).
14. Abduljaleel, Z. *et al.* Evidence of Trem2 variant associated with triple risk of alzheimer's disease. *PLoS One* **9**, (2014).

15. Menzies, G. E., Sims, R. & Williams, J. Molecular Dynamics simulations of Alzheimer's variants, R47H and R62H, in TREM2 provide evidence for structural alterations behind functional changes. *bioRxiv*, (2019).
16. Sudom, A. *et al.* Molecular basis for the loss-of-function effects of the Alzheimer's disease–associated R47H variant of the immune receptor TREM2. *Journal of Biological Chemistry* **293**, (2018).
17. Dash, R. *et al.* Dynamic insights into the effects of nonsynonymous polymorphisms (nsSNPs) on loss of TREM2 function. *Sci Rep* **12**, (2022).
18. Wang, Y. *et al.* TREM2 lipid sensing sustains the microglial response in an Alzheimer's disease model. *Cell* **160**, 1061–1071 (2015).
19. Zhao, Y. *et al.* TREM2 Is a Receptor for β-Amyloid that Mediates Microglial Function. *Neuron* **97**, (2018).
20. Zhong, L. *et al.* Amyloid-beta modulates microglial responses by binding to the triggering receptor expressed on myeloid cells 2 (TREM2). *Mol Neurodegener* **13**, (2018).
21. Bailey, C. C., Devaux, L. B. & Farzan, M. The triggering receptor expressed on myeloid cells 2 binds apolipoprotein E. *Journal of Biological Chemistry* **290**, 26033–26042 (2015).
22. Yeh, F. L., Wang, Y., Tom, I., Gonzalez, L. C. & Sheng, M. TREM2 Binds to Apolipoproteins, Including APOE and CLU/APOJ, and Thereby Facilitates Uptake of Amyloid-Beta by Microglia. *Neuron* **91**, (2016).
23. Atagi, Y. *et al.* Apolipoprotein E is a ligand for triggering receptor expressed on myeloid cells 2 (TREM2). *Journal of Biological Chemistry* **290**, (2015).
24. Kawabori, M. *et al.* Triggering receptor expressed on myeloid cells 2 (TREM2) deficiency attenuates phagocytic activities of microglia and exacerbates ischemic damage in experimental stroke. *Journal of Neuroscience* **35**, (2015).
25. Daws, M. R. *et al.* Pattern Recognition by TREM-2: Binding of Anionic Ligands. *The Journal of Immunology* **171**, (2003).
26. Cannon, J. P., O'Driscoll, M. & Litman, G. W. Specific lipid recognition is a general feature of CD300 and TREM molecules. *Immunogenetics* **64**, (2012).
27. Bruce, K. D., Zsombok, A. & Eckel, R. H. Lipid processing in the brain: A key regulator of systemic metabolism. *Frontiers in Endocrinology* vol. 8, (2017).
28. Loving, B. A. & Bruce, K. D. Lipid and Lipoprotein Metabolism in Microglia. *Frontiers in Physiology* vol. 11, (2020).
29. Li, R. Y. *et al.* TREM2 in the pathogenesis of AD: a lipid metabolism regulator and potential metabolic therapeutic target. *Molecular Neurodegeneration* vol. 17, (2022).
30. Kober, D. L. & Brett, T. J. TREM2-Ligand Interactions in Health and Disease. *J Mol Biol* **429**, 1607–1629 (2017).
31. Keren-Shaul, H. *et al.* A Unique Microglia Type Associated with Restricting Development of Alzheimer's Disease. *Cell* **169**, (2017).
32. Filipello, F. *et al.* Soluble TREM2: Innocent bystander or active player in neurological diseases? *Neurobiology of Disease* vol. 165, (2022).
33. Edwin, T. H. *et al.* A high cerebrospinal fluid soluble TREM2 level is associated with slow clinical progression of Alzheimer's disease. *Alzheimer's and Dementia: Diagnosis, Assessment and Disease Monitoring* **12**, (2020).
34. Franzmeier, N. *et al.* Higher CSF sTREM2 attenuates ApoE4-related risk for cognitive decline and neurodegeneration. *Mol Neurodegener* **15**, (2020).

35. Ewers, M. *et al.* Increased soluble TREM2 in cerebrospinal fluid is associated with reduced cognitive and clinical decline in Alzheimer's disease. *Sci Transl Med* **11**, (2019).
36. Suárez-Calvet, M. *et al.* sTREM 2 cerebrospinal fluid levels are a potential biomarker for microglia activity in early-stage Alzheimer's disease and associate with neuronal injury markers . *EMBO Mol Med* **8**, (2016).
37. Suárez-Calvet, M. *et al.* Early increase of CSF sTREM2 in Alzheimer's disease is associated with tau related-neurodegeneration but not with amyloid-β pathology. *Mol Neurodegener* **14**, (2019).
38. Park, S. H. *et al.* The relationship of soluble TREM2 to other biomarkers of sporadic Alzheimer's disease. *Sci Rep* **11**, (2021).
39. Brown, G. C. & St George-Hyslop, P. Does Soluble TREM2 Protect Against Alzheimer's Disease? *Frontiers in Aging Neuroscience* vol. 13, (2022).
40. Zhong, L. *et al.* Soluble TREM2 induces inflammatory responses and enhances microglial survival. *Journal of Experimental Medicine* **214**, (2017).
41. Zhong, L. *et al.* Soluble TREM2 ameliorates pathological phenotypes by modulating microglial functions in an Alzheimer's disease model. *Nat Commun* **10**, (2019).
42. Vilalta, A. *et al.* Wild-type sTREM2 blocks Aβ aggregation and neurotoxicity, but the Alzheimer's R47H mutant increases Aβ aggregation. *Journal of Biological Chemistry* **296**, (2021).
43. Varadi, M. *et al.* AlphaFold Protein Structure Database: Massively expanding the structural coverage of protein-sequence space with high-accuracy models. *Nucleic Acids Res* **50**, (2022).
44. Jumper, J. *et al.* Highly accurate protein structure prediction with AlphaFold. *Nature* **596**, (2021).
45. Šali, A. & Blundell, T. L. Comparative protein modelling by satisfaction of spatial restraints. *J Mol Biol* **234**, (1993).
46. Wu, E. L. *et al.* CHARMM-GUI membrane builder toward realistic biological membrane simulations. *Journal of Computational Chemistry* vol. 35, (2014).
47. Jo, S., Lim, J. B., Klauda, J. B. & Im, W. CHARMM-GUI membrane builder for mixed bilayers and its application to yeast membranes. *Biophys J* **97**, (2009).
48. Jo, S., Kim, T. & Im, W. Automated builder and database of protein/membrane complexes for molecular dynamics simulations. *PLoS One* **2**, (2007).
49. Lee, J. *et al.* CHARMM-GUI Membrane Builder for Complex Biological Membrane Simulations with Glycolipids and Lipoglycans. *J Chem Theory Comput* **15**, (2019).
50. Park, S., Choi, Y. K., Kim, S., Lee, J. & Im, W. CHARMM-GUI Membrane Builder for Lipid Nanoparticles with Ionizable Cationic Lipids and PEGylated Lipids. *J Chem Inf Model* **61**, (2021).
51. Brooks, B. R. *et al.* CHARMM: The biomolecular simulation program. *J Comput Chem* **30**, (2009).
52. Lee, J. *et al.* CHARMM-GUI Input Generator for NAMD, GROMACS, AMBER, OpenMM, and CHARMM/OpenMM Simulations Using the CHARMM36 Additive Force Field. *J Chem Theory Comput* **12**, (2016).
53. Bussi, G., Donadio, D. & Parrinello, M. Canonical sampling through velocity rescaling. *Journal of Chemical Physics* **126**, (2007).
54. Berendsen, H. J. C., Postma, J. P. M., Van Gunsteren, W. F., Dinola, A. & Haak, J. R. Molecular dynamics with coupling to an external bath. *J Chem Phys* **81**, (1984).

55. Parrinello, M. & Rahman, A. Polymorphic transitions in single crystals: A new molecular dynamics method. *J Appl Phys* **52**, (1981).
56. Abraham, M. J. *et al.* Gromacs: High performance molecular simulations through multi-level parallelism from laptops to supercomputers. *SoftwareX* **1–2**, (2015).
57. Hess, B., Bekker, H., Berendsen, H. J. C. & Fraaije, J. G. E. M. LINCS: A Linear Constraint Solver for molecular simulations. *J Comput Chem* **18**, (1997).
58. Andricioaei, I. & Karplus, M. Particle mesh Ewald: An N·log(N) method for Ewald sums in large systems The. *Statistical Mechanics of Fluid Mixtures The Journal of Chemical Physics* **115**, (2001).
59. Morris, G. M. *et al.* Software news and updates AutoDock4 and AutoDockTools4: Automated docking with selective receptor flexibility. *J Comput Chem* **30**, (2009).
60. Trott, O. & Olson, A. J. AutoDock Vina: Improving the speed and accuracy of docking with a new scoring function, efficient optimization, and multithreading. *J Comput Chem* **31**, (2010).
61. Eberhardt, J., Santos-Martins, D., Tillack, A. F. & Forli, S. AutoDock Vina 1.2.0: New Docking Methods, Expanded Force Field, and Python Bindings. *J Chem Inf Model* **61**, (2021).
62. Baker, N. A., Sept, D., Joseph, S., Holst, M. J. & McCammon, J. A. Electrostatics of nanosystems: Application to microtubules and the ribosome. *Proc Natl Acad Sci U S A* **98**, (2001).
63. Valdés-Tresanco, M. S., Valdés-Tresanco, M. E., Valiente, P. A. & Moreno, E. Gmx_MMPBSA: A New Tool to Perform End-State Free Energy Calculations with GROMACS. *J Chem Theory Comput* **17**, 6281–6291 (2021).
64. Miller, B. R. *et al.* MMPBSA.py: An efficient program for end-state free energy calculations. *J Chem Theory Comput* **8**, 3314–3321 (2012).
65. Duan, L., Liu, X. & Zhang, J. Z. H. Interaction entropy: A new paradigm for highly efficient and reliable computation of protein-ligand binding free energy. *J Am Chem Soc* **138**, 5722–5728 (2016).
66. Humphrey, W., Dalke, A. & Schulten, K. VMD: Visual molecular dynamics. *J Mol Graph* **14**, (1996).
67. Winkler, D. A. Ligand entropy is hard but should not be ignored. *Journal of Chemical Information and Modeling* vol. 60, (2020).
68. Polyansky, A. A., Zubac, R. & Zagrovic, B. Estimation of conformational entropy in protein-ligand interactions: A computational perspective. *Methods in Molecular Biology* **819**, (2012).
69. Chang, C. E. A., Chen, W. & Gilson, M. K. Ligand configurational entropy and protein binding. *Proc Natl Acad Sci U S A* **104**, (2007).
70. Ekberg, V. & Ryde, U. On the Use of Interaction Entropy and Related Methods to Estimate Binding Entropies. *J Chem Theory Comput* **17**, 5379–5391 (2021).
71. McQuade, A. *et al.* Gene expression and functional deficits underlie TREM2-knockout microglia responses in human models of Alzheimer's disease. *Nat Commun* **11**, (2020).
72. Wei, W. *et al.* TREM2 regulates microglial lipid droplet formation and represses post-ischemic brain injury. *Biomedicine and Pharmacotherapy* **170**, (2024).
73. Damisah, E. C., Rai, A. & Grutzendler, J. TREM2: Modulator of Lipid Metabolism in Microglia. *Neuron* vol. 105, (2020).
74. Nagata, S., Suzuki, J., Segawa, K. & Fujii, T. Exposure of phosphatidylserine on the cell surface. *Cell Death and Differentiation* vol. 23, (2016).

75. Fassler, M., Benaim, C. & George, J. TREM2 Agonism with a Monoclonal Antibody Attenuates Tau Pathology and Neurodegeneration. *Cells* **12**, (2023).
76. Schlepckow, K. *et al.* Enhancing protective microglial activities with a dual function TREM 2 antibody to the stalk region . *EMBO Mol Med* **12**, (2020).
77. van Lengerich, B. *et al.* A TREM2-activating antibody with a blood–brain barrier transport vehicle enhances microglial metabolism in Alzheimer's disease models. *Nat Neurosci* **26**, (2023).